

Simulating the Hamiltonian of Dimer Atomic Spin Model of One Dimensional Optical Lattice on Quantum Computers

Sudev Pradhan,^{1,*} Amlandeep Nayak,^{1,†} Sritam Kumar Satpathy,^{1,‡} Tanmaya Shree Behera,^{1,§} Ankita Misra,^{2,¶} Debashis Swain,^{2,**} and Bikash K. Behera^{3,††}

¹*Department of Physical Science,
Indian Institute of Science Education and Research, Berhampur, 760010, Odisha, India*

²*Department of Chemical Science,
Indian Institute of Science Education and Research, Berhampur, 760010, Odisha, India*

³*Department of Physical Sciences,
Indian Institute of Science Education and Research Kolkata, Mohanpur 741246, West Bengal, India*

Abstract

The one-dimensional Ising model with its connections to several physical concepts plays a vital role in comprehension of several principles, phenomena and numerical methods. The Hamiltonian of a coupled one-dimensional dissipative spin system in the presence of magnetic field can be obtained from the Ising model. We simulate the above Hamiltonian by designing a quantum circuit with precise gate measurement and execute with the IBMQ experience platform through different N states with controlled energy separation where we can check quantum synchronization in a dissipative lattice system. Our result shows the relation between various entangled states, the relation between the different energy separation (ω) with the spin-spin coupling (λ) in the lattice, along with fidelity calculations for several iterations of the model used. We also estimate the ground and first excited energy states of Ising-Hamiltonian using VQE algorithm and investigate the lowest energy values varying the number of layers of ansatz.

I. INTRODUCTION

Quantum advantage refers to the ability of quantum computers to solve problems at a faster rate than classical computers while utilizing reduced resources. In the 21st century there has been great progress towards establishment and progress of quantum advantage through demonstration of Shor's algorithm^{1,2} and implementation of Deutsch's algorithm³⁻⁵ through use of clustered quantum computers. However, the complexity required to build a quantum computer retaining all the advantages granted by quantum computation is impossible to attain with current technology. Hence, several sub universal models which retain parts of total advantage of quantum computation have been realized, use of which are widespread. These sub universal models are assigned to specific problems which are difficult to solve utilising classical machines, thereby demonstrating quantum advantages on several different aspects.

The quantum spin systems and the study of its lower energy model could be done by the ultra-cold atoms^{6,7} and this spin systems help us to explore more about the quantum phase transition, entanglement and other many body theoretical models⁸⁻¹¹. In order to get the desired effects or phenomenon in spin systems we need to minimise the degree of freedom of the coupling state, which would otherwise result collective dissipation and lead to destruction of quantum states. We have consider dimer atomic bosonic species with one dimensional optical lattice because this ultra-cold bosonic species serves best to simulate the Hamiltonian of the Ising spin model¹²⁻¹⁷. Here we use Ising Model equivalent of a dimer atomic lattice to learn of its Hamiltonian and its

eigenvalue solutions¹⁸. The Ising model of today is concerned with the physics of phase transitions, which occur when a small change in a parameter such as temperature or pressure causes a large-scale, qualitative change in the state of a system. Ising model starts with equally spaced points in a lattice of any dimension where each point has a spin of $\frac{1}{2}$ or $-\frac{1}{2}$. These points are independent and show coupling interaction due to mean/average fields of neighbouring spins. One purpose of the Ising model is to explain how short-range interactions¹⁹ between, say molecules in a crystal give rise to long-range, correlative behavior, and to predict in some sense the potential for a phase transition²⁰. The Ising model has also been applied to problems in chemistry²¹, molecular biology²², and other areas where "cooperative" behavior of large systems is studied. Phase separation is one of the first facets where Ising model was used, it investigated spontaneous magnetization in ferromagnetic film (i.e. magnetization in the absence of external magnetic field) Transition temperature depends on the strength of the inter-spin exchange coupling, concepts of Ising model help in studying phase separation in binary alloys²³ and liquid-gas phase transitions²⁴.

Solving the Hamiltonian in this 1D optical lattice would also help us to study quantum synchronisation. We understand Synchronization as "adjustment of rhythms of the oscillating object due to their weak interaction"²⁵ but in quantum state synchronizing a clock²⁶ with quantum variables when the information is passed to two different person which might have different phase and state²⁷ or the reduction of noise. This synchronisation is useful in steady super radiant emission^{28,29} in the harmonic oscillator. We can see this quantum syn-

chronization in these atomic systems with the help of collective gratification coupling with the atoms and all because of super-radiance³⁰ of incongruous effects.

To solve this dissipative Ising-Hamiltonian and getting its eigenvalue along with its energy levels we use Variational quantum eigensolver (VQE). The VQE method was introduced to mitigate the significant hardware demands needed by the QPE (quantum phase estimation) approach. VQE is a hybrid quantum-classical algorithm, where the computational workload is shared between available classical and quantum resources³¹. It starts with a reasonable assumption about the form of the target wave function with the ground state trial wave function being generated from operators that result in single and double-excitation configurations from Hartree-Fock wave function³² which is precomputed on a classical computer. Next, on a quantum computer, the trial wave function is prepared and the expectation value of the Hamiltonian is measured. Then, the parameters of the trial wave function are optimized iteratively on a classical computer using the variational principle³³.

VQE⁴⁶ provides eigen-solutions for trail ground state and first excited state wavefunctions. The ground and excited state energy are then plotted through several graphs to check their general trend, their dependency on several individual operators used as gates and to check a general maxima or minima of the energy eigenvalues.

In the following sections we show how to apply the prior mentioned portions. Specifically, we show how to implement Ising-Hamiltonian on IBM Quantum computer by setting up intermediate circuit and performing several observations on different relations such as that of:

- Time correlation and average value using different values for spin spin interaction term⁴⁷/coupling constant.
- Different energy separations and coupling constant.

Fidelity calculation⁴⁸ for the circuit is also done by using the data obtained by computing the circuit both classically and with quantum computers. Eigen-solutions for the Ising-Hamiltonian is also obtained using VQE, we have also included several plots displaying the relation (i) of energy with number of layers, and (ii) of energy with changing external field intensity, in order to better explain various trends of the obtained energy.

II. THEORY

Super cold atom in atomic lattice³⁴ is perfect to simulate the Hamiltonian spin³⁵ complex where we can implement by two different techniques i.e. optical driving of two hyperfine levels³⁶ and interacting with the Ising spin³⁷ of mott-insulator³⁸. Using the later technique we simulate the Hamiltonian Operator with the effective spin of a single atom where they are restricted to each lattice potential and this lattice potential is localised and basic

ground states and excited states are marked as $|0\rangle$ and $|1\rangle$ and a effective spin of $\frac{1}{2}$ in each lattice where these collective atoms work in a restricted region. With the use of lattice potential³⁹ we can state the disintegration of atoms which ultimately end up, cooling of the system. When we simulate this spin system the ground state is achieved faster than the excited states and thus it will eliminate the excited states which will reduce to desired 2 level system. The simple Hamiltonian by the optical coupling is mentioned in the qualitative description in the paper⁴⁰. This sets up the equation for a two level system as:

$$\dot{\rho}_t = \sum_k A^- (2\sigma_k^- \rho_t \sigma_k^+ - \{\sigma_k^+ \sigma_k^-, \rho_t\}_+) - i[H, \rho_t]. \quad (1)$$

where, $\sigma_k^- = (\sigma_k^+)^{\dagger}$, $\sigma_k^+ = |1\rangle\langle 0|_k$ and A^- indicates the terms of decay as mentioned in⁴⁰.

And using this main equation from this⁴¹ paper and considering all level of the atomic lattice and coupled through a detuned Raman transition⁴² by passing through the excited state and we obtain the Fourier integral of the Hamiltonian states⁴³ containing discrete staggered energy states and the spin spin coupling (λ).

Assuming the on-site interaction, a single potential well consist of 2 atoms, where we can use the perturbation theory. Implementing this dissipative model technique and double well we can reduce the Hamiltonian Operator to a summation of staggered energy of the lattice dimer with the coupling complex and magnetic field in z-direction and tunable transverse field. In this XXZ spin chain model, if we don't consider the z-direction of magnetic field, it would effectively calculate the steady state dynamics. And we consider the time dependent equation for the x direction of magnetic field for the equation (1) as mentioned in the dissipative spin chain section of⁴⁰ so using the perturbation theory and the given manipulation the optical well and we can sum up the Hamiltonian as follows:-⁴¹

$$\hat{H} = \sum_{j=1}^N \frac{\omega_j}{2} \hat{\sigma}_j^z + \sum_{j=1}^{N-1} \lambda (\hat{\sigma}_j^+ \hat{\sigma}_{j+1}^- + h.c.), \quad (2)$$

where $\omega_0 \gg \omega_{1,2}, \delta, \lambda$, where $\delta = \omega_1 - \omega_2$ ¹ is the detuned coefficient of the lattice potential and ($\hbar = 1$).

In order to reduce the Hamiltonian into a quantum circuit, we take the simplest state for $N = 2$, (2 qubit system), and construct the circuit. Similarly for the next iteration of N, it follows the same trend. We apply the time evolution unitary operator⁴⁴ on our Hamiltonian to get,

$$U(t) = e^{-\frac{i\hat{H}t(2\pi)}{\hbar}} \quad (3)$$

where t refers to time and \hat{H} is the combination of H_1 and H_2 , where $H_1 = \sum_{j=1}^N \frac{\omega_j}{2} \hat{\sigma}_j^z$ and $H_2 = \sum_{j=1}^{N-1} \lambda (\hat{\sigma}_j^+ \hat{\sigma}_{j+1}^- + h.c.)$ but due to the presence of

$\lambda(\sigma_x\sigma_x + \sigma_y\sigma_y)$, it does not allow these two Hamiltonian to commute, $[H_1, H_2] \neq 0$ ⁴⁵, hence we use totom decomposition and by taking $\frac{h}{2\pi} = 1$ we could write the equation as

$$U(t) = [(e^{-\frac{iH_1 t}{n}}).(e^{-\frac{iH_2 t}{n}})]^n \quad (4)$$

where $\frac{t}{n}$ is the small interval which we can write as Δt and our above equation will be modified to

$$U(t) = [(e^{iH_1 \Delta t}).(e^{iH_2 \Delta t})]^n \quad (5)$$

where we will repeat the process n times or theoretically we will iterate our quantum circuits n number of times. As the value of n increases we will get more accurate results. Now substituting the value of H_1 and H_2 in the above equation (5), we get

$$U(t) = [(e^{i(\frac{\omega_j}{2}\hat{\sigma}_j^z)\Delta t}).(e^{i\lambda(\hat{\sigma}_j^+\hat{\sigma}_{j+1}^-)\Delta t})]^n \quad (6)$$

where, $\sigma^x = \begin{bmatrix} 0 & 1 \\ 1 & 0 \end{bmatrix}$, $\sigma^y = \begin{bmatrix} 0 & -i \\ i & 0 \end{bmatrix}$ and $\sigma^z = \begin{bmatrix} 1 & 0 \\ 0 & -i \end{bmatrix}$
⁴⁹ Dividing the equation (6) into 2 parts as -

$$U_a(t) = [e^{i(\frac{\omega_j}{2}\hat{\sigma}_j^z)\Delta t}]^n \quad (7)$$

$$U_b(t) = [e^{i\lambda(\hat{\sigma}_j^+\hat{\sigma}_{j+1}^-)\Delta t}]^n \quad (8)$$

On solving the equation (7) (the first part of the equation) and assuming for a single iteration ($n=1$) and this follows the condition of⁵⁰

$$e^{-i\theta A} = \cos(\theta)I - i\sin(\theta)A \quad (9)$$

where I is the identity matrix and A is of same order of the identity matrix where $A^2 = I$. Here, $A = \sigma_z$, which follow the identity rule($\sigma_z^2 = I$) which has a order 2, and $\theta = \frac{\omega_j \Delta t}{2}$, substituting this, we get

$$U_a(t) = \cos(\frac{\omega_j \Delta t}{2})I - i\sin(\frac{\omega_j \Delta t}{2})\sigma_z \quad (10)$$

under matrix transformation,

$$U_a(t) = \begin{bmatrix} e^{-\frac{i\omega_j \Delta t}{2}} & 0 \\ 0 & e^{\frac{i\omega_j \Delta t}{2}} \end{bmatrix} = \exp \frac{-i\omega_j \Delta t}{2} \begin{bmatrix} 1 & 0 \\ 0 & e^{i\omega_j \Delta t} \end{bmatrix} \quad (11)$$

this $U_a(t)$ matrix represent a similar matrix of $U1$ gate on IBMQ where $U1(\theta t)$ is replace by $U1(\omega_j \Delta t)$ and

according to our Hamiltonian ω is flexible. So applying $U1$ gate on first qubit satisfy $j=1$ term where $U1(\omega_1 \Delta t)$ and same goes with the another qubit for $j=2$, we get another $U1(\omega_2 \Delta t)$ gate and goes on till N . But in order for the $U1$ gate to work we need a Hadamard gate in order to produce a superposition state which will activate the $U1$ gate as in Fig: 1

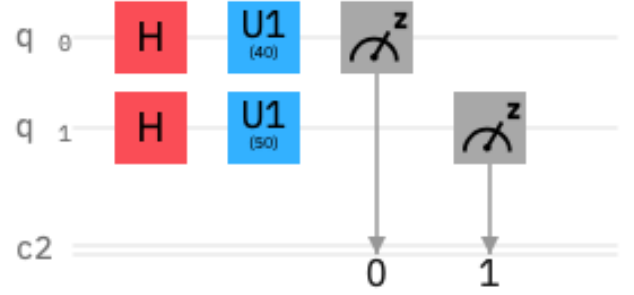


FIG. 1: Circuit describing H gate with $U1$ gate on $q[0]$ qubit where $U1$ gate has $\omega_1 t$ as $\frac{\pi}{2}$ where we get a entangled state.

Similarly, working for the equation (8) we get a reduced matrix format which on solving the later part of the equation, $e^{i\lambda(\hat{\sigma}_j^+\hat{\sigma}_{j+1}^-)\Delta t}$, with considering as $\sigma^+ = \sigma_x + i\sigma_y$ and $\sigma^- = \sigma_x - i\sigma_y$ which reduce down the equation to $e^{\lambda(\sigma_x\sigma_x + \sigma_y\sigma_y)\Delta t}$ or can be written as $e^{\lambda(\sigma_x\sigma_x)\Delta t}e^{(\sigma_y\sigma_y)\Delta t}$ and solving the $e^{\lambda\Delta t(\sigma_x\sigma_x)}$ in a Euler formula⁵⁰, we get

$$e^{-i\theta B} = \cos(\theta)I - i\sin(\theta)B \quad (12)$$

where I is the identity matrix and B is of same order of the identity matrix.

Here, $B = \sigma_x \otimes \sigma_x$, which follow the identity rule and has a order 4 and $\theta = \lambda\Delta t$, substituting this, we get

$$U_1(t) = \cos(\lambda\Delta t)I - i\sin(\lambda\Delta t)\sigma_x \otimes \sigma_x \quad (13)$$

And converting to the matrix format,

$$\begin{bmatrix} \cos(\lambda\Delta t) & 0 & 0 & -i\sin(\lambda\Delta t) \\ 0 & \cos(\lambda\Delta t) & -i\sin(\lambda\Delta t) & 0 \\ 0 & -i\sin(\lambda\Delta t) & \cos(\lambda\Delta t) & 0 \\ -i\sin(\lambda\Delta t) & 0 & 0 & \cos(\lambda\Delta t) \end{bmatrix} \quad (14)$$

which shows a normal $U3(\theta, -\frac{\pi}{2}, \frac{\pi}{2})$ on IBMQ where θ varies according to $\lambda\Delta t$ vary. Where $U3$ gate controls The three parameters allowing the construction of any single-qubit gate, has a duration of one unit of gate time. In the Bloch sphere rotation⁵¹, it can move through

any plane controlled by $(\theta, \gamma$ and $\phi)$ only once and its matrix form is represented by

$$\begin{bmatrix} \cos(\frac{\theta}{2}) & -e^{i\lambda}\sin(\frac{\theta}{2}) \\ e^{i\phi}\sin(\frac{\theta}{2}) & e^{i(\phi+\lambda)}\cos(\frac{\theta}{2}) \end{bmatrix}$$

hence putting two CNOT gates i.e.

$$\begin{bmatrix} 1 & 0 & 0 & 0 \\ 0 & 1 & 0 & 0 \\ 0 & 0 & 0 & 1 \\ 0 & 0 & 1 & 0 \end{bmatrix}$$

and $U3$ with defined parameter in between, we can obtain the result of the above matrix of $U1$. Hence, solving the matrix and comparing it with the $U3$ matrix we derive the following circuit as in Fig. 2:

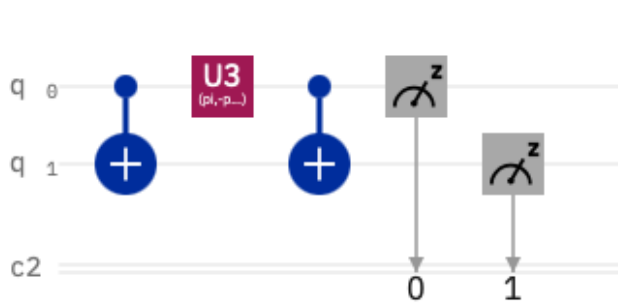


FIG. 2: The derived circuit has a combination of a CNOT gate, $U3$ gate and a CNOT gate, where $\theta = \lambda\Delta t$, $\phi = -\pi/2$ and $\lambda = \pi/2$.

Similar the second part of (8), $\lambda\Delta t(\sigma_y\sigma_y)$ we could calculated as,

$$U_b(t) = \cos(\lambda\Delta t)I - i\sin(\lambda\Delta t)\sigma_y \otimes \sigma_y$$

$$\begin{bmatrix} \cos(\lambda\Delta t) & 0 & 0 & i\sin(\lambda\Delta t) \\ 0 & \cos(\lambda\Delta t) & -i\sin(\lambda\Delta t) & 0 \\ 0 & -i\sin(\lambda\Delta t) & \cos(\lambda\Delta t) & 0 \\ i\sin(\lambda\Delta t) & 0 & 0 & \cos(\lambda\Delta t) \end{bmatrix} \quad (15)$$

similarly on solving this matrix manually, we get a combination of control $U3$ and anti control $U3$ matrix, where control $U3$ is a 4×4 matrix $(I \otimes |0\rangle\langle 0| + U3 \otimes |1\rangle\langle 1|)$ i.e.

$$\begin{bmatrix} 1 & 0 & 0 & 0 \\ 0 & \cos(\frac{\theta}{2}) & 0 & -e^{i\lambda}\sin(\frac{\theta}{2}) \\ 0 & 0 & 1 & 0 \\ 0 & e^{i\phi}\sin(\frac{\theta}{2}) & 0 & e^{i(\phi+\lambda)}\cos(\frac{\theta}{2}) \end{bmatrix}$$

and anti control $U3$ is also a 4×4 matrix $(I \otimes |1\rangle\langle 1| + U3 \otimes |0\rangle\langle 0|)$ i.e.

$$\begin{bmatrix} \cos(\frac{\theta}{2}) & 0 & -e^{i\lambda}\sin(\frac{\theta}{2}) & 0 \\ 0 & 1 & 0 & 0 \\ e^{i\phi}\sin(\frac{\theta}{2}) & 0 & e^{i(\phi+\lambda)}\cos(\frac{\theta}{2}) & 0 \\ 0 & 0 & 0 & 1 \end{bmatrix}$$

and placing this combination of matrix within 2 CNOT matrix with specified value of (θ, γ, ϕ) we get the above matrix.

Where the equivalent matrix is reduced in the form of circuit, as per Fig. 3.

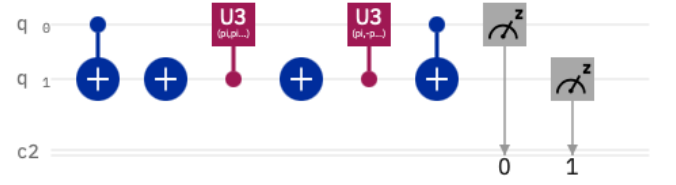


FIG. 3: The derived circuit has a combination of a CNOT gate, control $U3$ gate, Anti-control $U3$ gate and a CNOT gate, where $\theta_1 = \lambda\Delta t$, $\phi_1 = -\pi/2$ and $\lambda_1 = \pi/2$ and $\theta_2 = \lambda\Delta t$, $\phi_2 = \pi/2$ and $\lambda_2 = -\pi/2$.

and summing up all the circuits for $N=2$, we can add all the circuits together and as we know that two CNOT gates are equal to identity matrix so we can omit that and the resulting circuit somewhat looks like this as in Fig. 4.

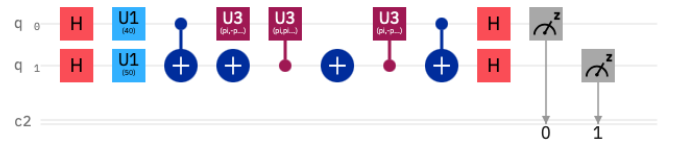


FIG. 4: The equivalent circuit describes the Hamiltonian operator 2 in a $N=2$ state.

We can say the following matrices are the Ising matrices⁵² which confirm the Ising spin complex of the atom in the lattice potential.

III. IMPLEMENTATION ON IBM QUANTUM EXPERIENCE

A. Setting up the intermediate circuit

The primary task is to implement the above constraint as the unitary time evolution operator⁴⁴, which we have done through implementing through $U1$, $U3$ and $U3^\dagger$

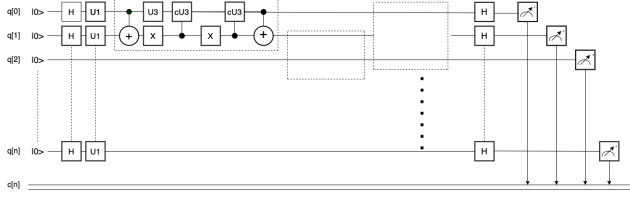


FIG. 5: The skeletal body of the general circuit for N qubits.

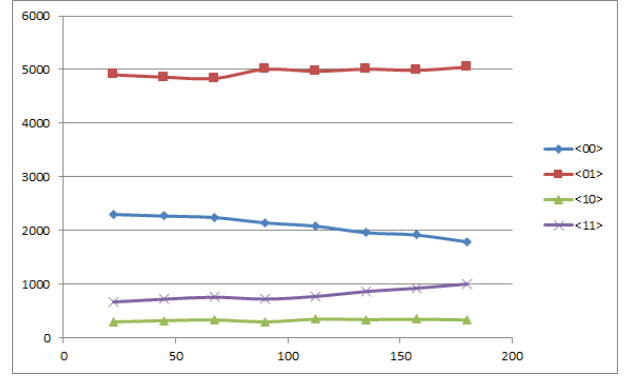
gates by controlling their measures and converting them to the basic quantum circuit so that the phase is not disturbed. We set the parameters θ , ϕ and λ as per our requirement to simulate \hat{H} .

Setting the (III) as a basic circuit on IBM Q as implementing the simple $U1$ gate along with the measurement gate, If we choose θ as $\frac{\pi}{2}$, $q[0]$ gives $|0\rangle$ and $q[1]$ gives $|1\rangle$ and we use the Hadamard gate along with $U1$ gate we get a superposition of the two states $|0\rangle |1\rangle$ as in fig:1. In the above equation (2) with the precise measurement $\omega_1 t$ we can get the synchronized state.

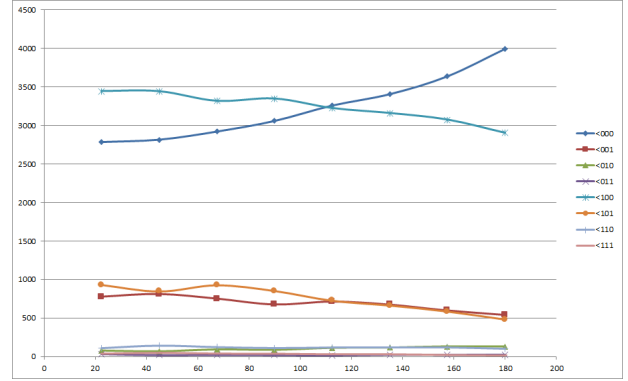
In the Fig: 6 and 7c is for $N=2$ showing the percentage of each state in both classical simulators and real quantum machine respectively with the desired result which shows the entanglement.

Similarly, we set the second part of the equation (2), by applying the unitary time evolution operator, we get $U3$ and $U3^\dagger$ gates with precise measurement of θ , ϕ and λ ; where ϕ and λ are $-\frac{\pi}{2}$ and $\frac{\pi}{2}$ respectively for $U3$ gate where as ϕ and λ are $\frac{\pi}{2}$ and $-\frac{\pi}{2}$ respectively for $U3^\dagger$ gate. Adding the following information we can reduce the quantum circuits as Fig: 4 with the desired entangled state probability as in Fig: 6 and 7c. The general skeletal body of the Hamiltonian Operator with defined value of θ , ϕ and λ as in Fig: 5.

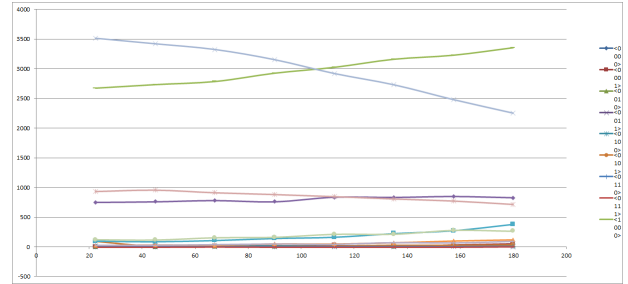
When simulating the Hamiltonian Operator for N states we get a result as in Fig: 7 with each N state with varying λt , which shows different entangled states for particular degree radian.



(a)



(b)

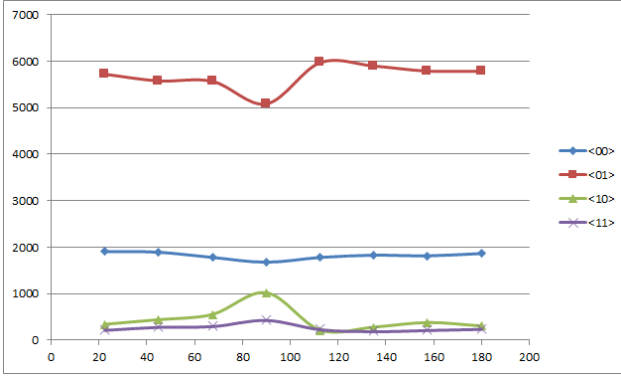


(c)

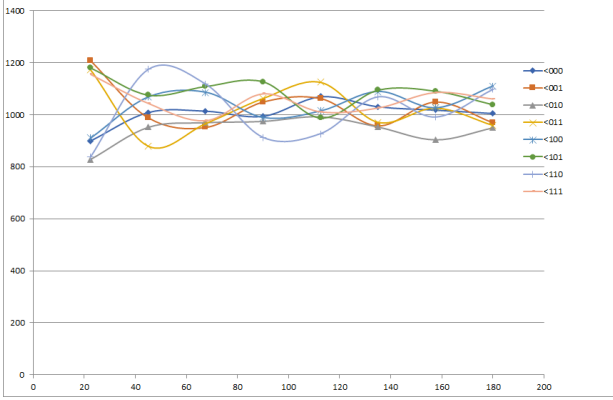
FIG. 6: **Simulation results for probabilities of each state.**(a) When $N=2$ (b) $N=3$ (c) $N=4$ and (d) $N=5$; it shows the variation in probability of each state with respect to λt , where λt is in term of degree radian and the y axis shows the percentage probability and each line indicate each entangled state with N qubits.

B. Time correlation and the Average value

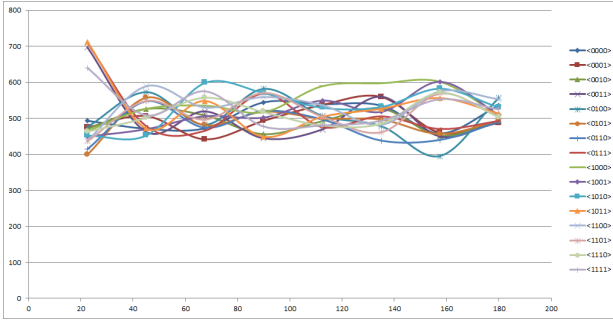
When we take in option with two or more than two body system we are introduced by a factor called phase locking⁵³ but this one-time correlation indeed help us to see the relationship between the average value and its weak dependence on λ which is a condition for the synchronizing states. This average value somewhere depends on particular eigenvalue or particular spin



(a)



(b)



(c)

FIG. 7: **Quantum computer results for probabilities of each state.**(a) When N=2 (b) N=3 (c) N=4 and (d) N=5; it shows the variation in probability of each state with respect to λt , where λt is in term of degree radian and the y axis shows the percentage probability and each line indicate each entangled state with N qubits.

quantum number⁵⁴. While calculating the average value we can see the overlapping of the states which could be concluded as the opposite spin states. We observe the resonance peaks of the synchronized⁵⁵ and the rest other eigenstates, where we can also observe the relation between λ and ω .

To show this variation of weak dependence of spin quantum number on the average value and its depen-

dence, we make a circuit that depicts the average value of each Pauli's matrices. These circuits also depict the relation between the λ and ω for each excited state in the synchronization system. These synchronized states depend on many body or many-time correlation function, dependency on time is very low.

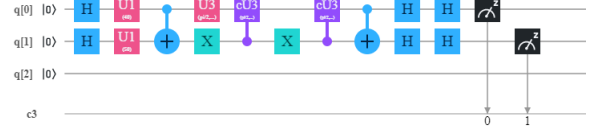


FIG. 8: Circuit representation of the average value of $\langle \sigma_x | \sigma_x \rangle$ when N=2 state adding a H gate at the end of the main circuit representing the operator.

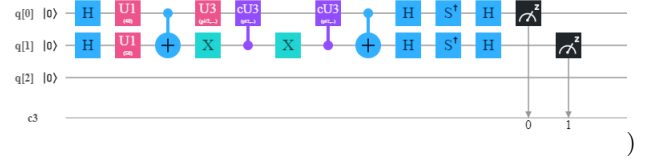


FIG. 9: Circuit representation of the average value $\langle \sigma_y | \sigma_y \rangle$ when N=2 state keeping S^\dagger and H gate at end.

Here, we would show the circuit of the average value of $\langle \sigma_x | \sigma_x \rangle$ in Fig: 8 by connecting another Hadamard gate.

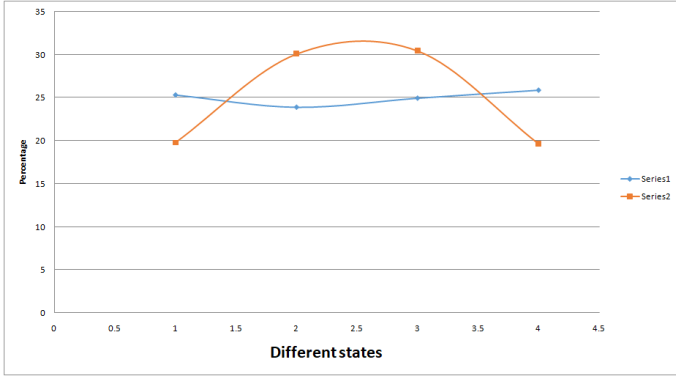
at the end of the circuit with a particular θ as $\frac{\pi}{2}$ and rest other coefficient for the $U3$, ϕ and λ as $-\frac{\pi}{2}$ and $\frac{\pi}{2}$ respectively and $U3^\dagger$, ϕ and λ as $\frac{\pi}{2}$ and $-\frac{\pi}{2}$ respectively.

Similarly, $\langle \sigma_y | \sigma_y \rangle$ are the average value which depicts the time correlation function. We can theoretically obtain this by showing the excitation state overlapping with the other eigen value, but in quantum circuit wise, we can show them by using a S^\dagger followed by a Hadamard gate at the end of the circuit Fig: 9 where θ as $\frac{\pi}{2}$ and rest other coefficient for the $U3$ and $U3^\dagger$ gate remain the same.

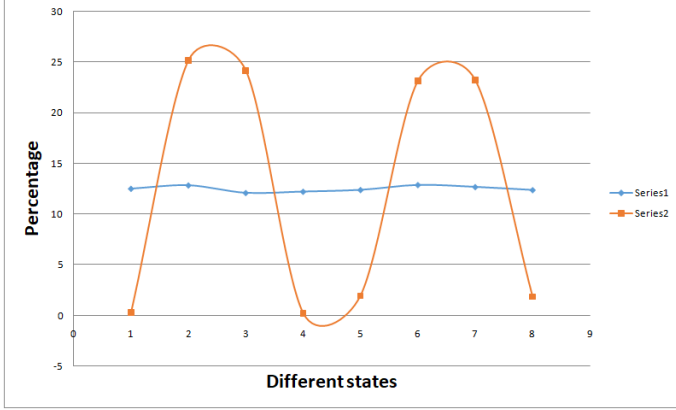
Merging all this information we could relate the data from Fig: 10, where we have simulated N=2 to N=4.

C. Relation between the different energy separation (ω) with the spin-spin coupling (λ)

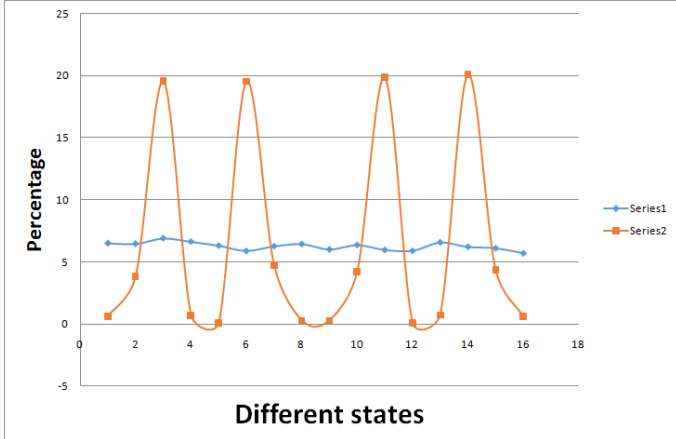
As per the dissipative state⁴⁰, we can have different ω (transverse field term) in Ising-Hamiltonian for different lattice points. This along with the spin spin coupling⁵⁶ constant are necessary in order to complete the Hamiltonian. In order to check any relation between these terms we have varied θ values of either U gate while keeping the other constant, the λt thereby the theta for $U3$ gate is changed regularly irrespective of the changes in ω . The results obtained is plotted for various constant values of different ω in Fig: 11 and 12.



(a)



(b)



(c)

FIG. 10: **Variation of probabilities of different states in x and y basis.** (a) When $N=2$ (b) $N=3$ and (c) $N=4$; it shows the average value of each state (blue line representing $\langle \sigma_x | \sigma_x \rangle$ and red line representing $\langle \sigma_y | \sigma_y \rangle$) for particular $\lambda t = \frac{\pi}{2}$ where we can check the overlapping value of the particular eigenstate and we could also check the resonance peak.

Here, we find the synchronised state of the system for a particular ω and λ . From the provided plots, it can be

easily observed that results due to ω_2 remaining as constant is not much affected by varying λt whereas results due to ω_1 remaining as constant shows drastic change with varying λt with the probabilities showing different change pattern for different states.

IV. VARIATIONAL QUANTUM EIGENSOLVER

VQE⁴⁶ is a hybrid module using both quantum and classical resources to find expectation values of H , where H is the Hamiltonian of the entire system when run in quantum simulations such as in this case. For VQE a quantum subroutine is run inside of a classical optimization loop, in two fundamental steps:

- Prepare the quantum state $|\psi(\vec{\theta})\rangle$ often called then ansatz.
- Measure the expectation value $\langle \psi(\vec{\theta}) | H | \psi(\vec{\theta}) \rangle$

The trial quantum state/parametrized state (or ansatz) preparation can be tricky, the algorithms need to be considered carefully since it can dramatically affect performance. By arbitrarily selecting a wave function $|\psi\rangle$ (called an ansatz) as an initial guess, approximating it as $|\psi_{min}\rangle$, calculating its expectation value, $\langle \psi | H | \psi \rangle$ and iteratively updating the wave function, arbitrarily tight bounds on the ground state energy of a Hamiltonian may be obtained. The variational principle⁵⁷ ensures that this expectation value is always greater than the smallest eigenvalue of H .

For this particular case we have used a simplified ansatz of $U3$ gates. A simplified form of it can be shown:

$$\left. \begin{array}{l} |\psi_0\rangle \xrightarrow{U3(\theta_0, \phi_0, \lambda_0)} \oplus \xrightarrow{U3(\theta_2, \phi_2, \lambda_2)} \bullet \xrightarrow{U3(\theta_4, \phi_4, \lambda_4)} \oplus \xrightarrow{U3(\theta_6, \phi_6, \lambda_6)} \\ |\psi_1\rangle \xrightarrow{U3(\theta_1, \phi_1, \lambda_1)} \bullet \xrightarrow{U3(\theta_3, \phi_3, \lambda_3)} \oplus \xrightarrow{U3(\theta_5, \phi_5, \lambda_5)} \bullet \xrightarrow{U3(\theta_7, \phi_7, \lambda_7)} \end{array} \right\} |\psi'\rangle$$

This ansatz is just limited to 3 parameters and hence can be efficiently optimized. It is to be understood that the capacity to create an arbitrary state guarantees that during the optimization process, the variational form

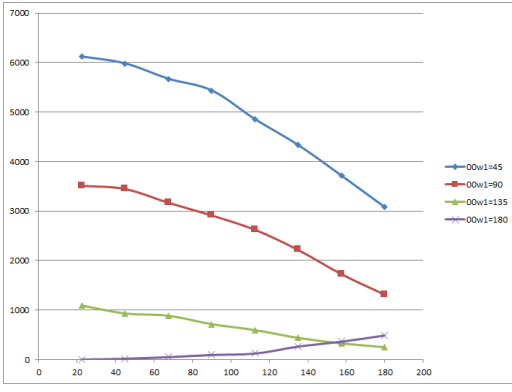
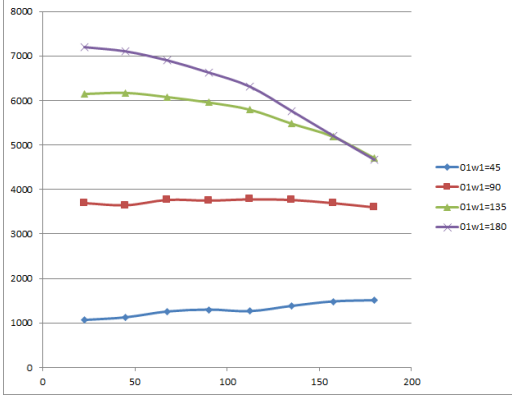
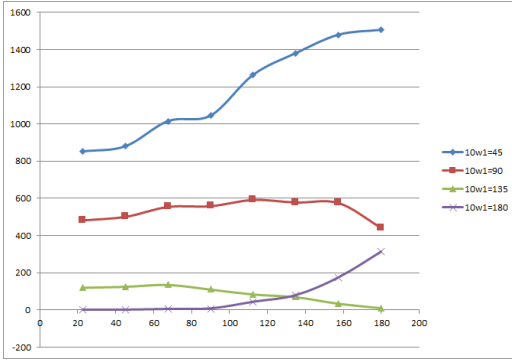
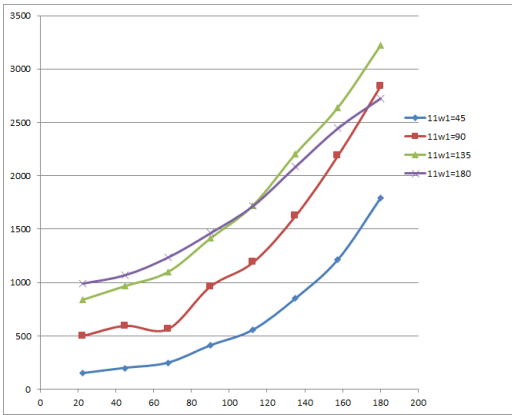
(a) '00' for constant values of ω_1 (b) '01' for constant values of ω_1 (c) '10' for constant values of ω_1 (d) '11' for constant values of ω_1

FIG. 11: Variation of probabilities for different states with λ for constant values of ω_1 while ω_2 varies for $N=2$. (a) '00' (b) '01' (c) '10' (d) '11'

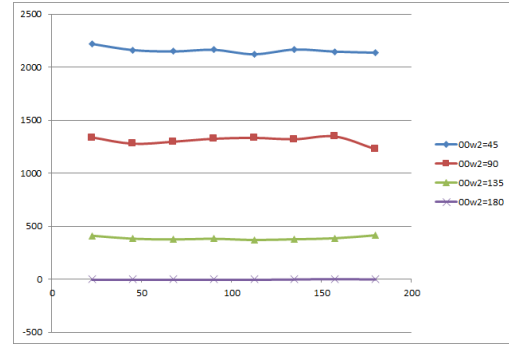
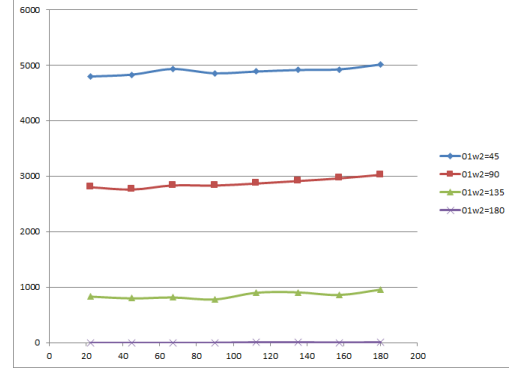
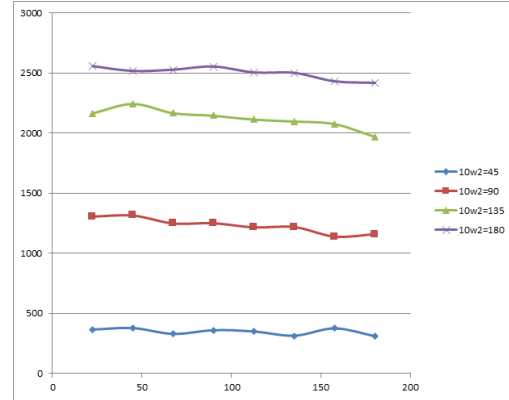
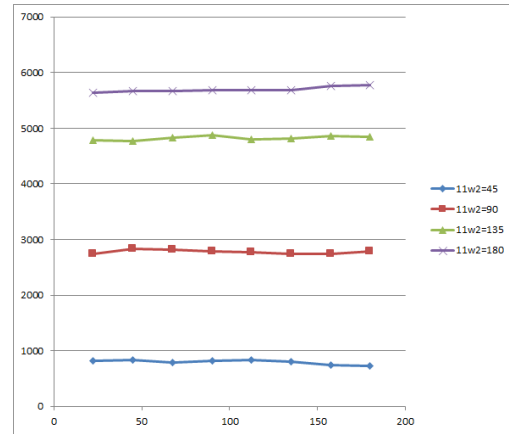
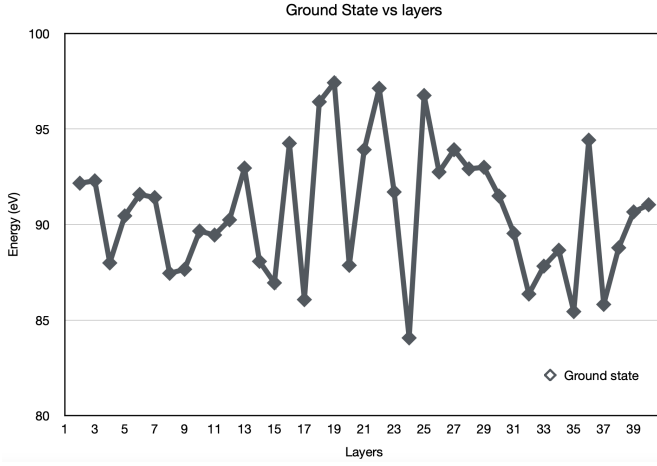
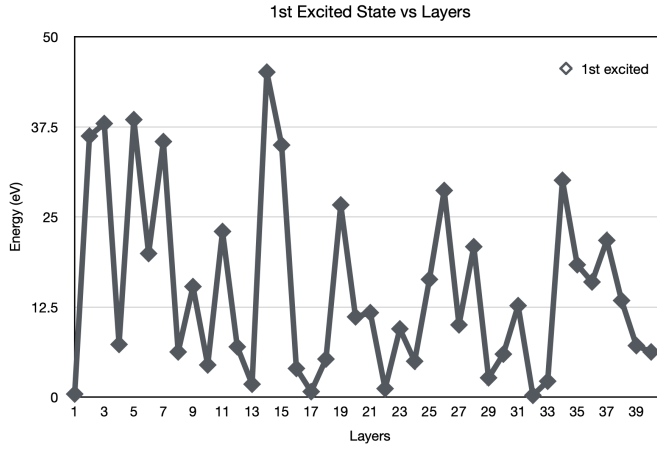
(a) '00' for constant values of ω_2 (b) '01' for constant values of ω_2 (c) '10' for constant values of ω_2 (d) '11' for constant values of ω_2

FIG. 12: Variation of probabilities for different states with λ for constant values of ω_2 while ω_1 varies for $N=2$. (a) '00' (b) '01' (c) '10' (d) '11'



(a) Variation of Ground State Energy

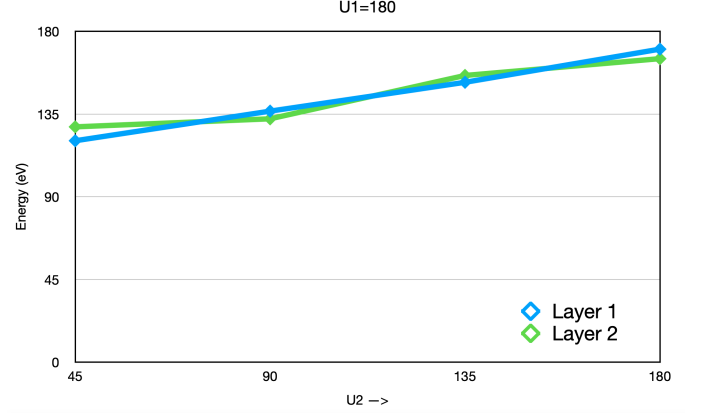


(b) Variation of 1st Excited State Energy

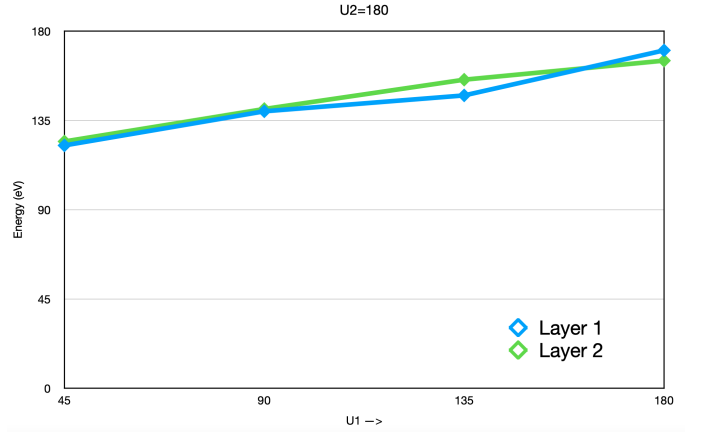
FIG. 13: Variation of both eigensolutions for Ising-Hamiltonian across 40 layers. (a) Ground State (b) 1st Excited State

doesn't restrict the number of achievable states over which the expectation value of H can be taken. In return this ensures that the minimum expectation value is limited only by the capabilities of the classical optimizer.

For classical optimizer we have opted to use the Simultaneous Perturbation Stochastic Approximation optimizer (SPSA) optimizer⁵⁸. It is an appropriate optimizer for optimizing a noisy objective function. SPSA approximates the gradient of the objective function with only two measurements. It does so by simultaneously perturbing all of the parameters in a random fashion, rather than the gradient descent where each parameter is perturbed independently. While using VQE in either a noisy simulator⁵⁹ or on real hardware, SPSA is used as the recommended classical optimizer.



(a) ω_1 remains constant



(b) ω_2 remains constant

FIG. 14: Variation in probabilities of different states with for constant values of either ω while other varies for $N=2$. (a) ω_1 constant with $U1=\pi$ (b) ω_2 constant with $U2=\pi$

With the defined ansatz and classical optimizer, we use VQE and obtain both the minimum ground state and 1st excited state energies for various layers of ansatz, all of which are plotted in Fig: 13. Couple of graphs (Fig: 14) comparing ground state energy in different layers with varying ω have been shown. From Fig: 14 no concrete pattern for the peaks and troughs of different energy states with respect to layers could be found.

V. FIDELITY

Fidelity⁴⁸ is the measure of closeness between two quantum states. In our case, ψ_ρ is the measured state and ψ_σ is the pure quantum state. Let's define two density matrices such as $\rho = |\psi_\rho\rangle\langle\psi_\rho|$ and $\sigma = |\psi_\sigma\rangle\langle\psi_\sigma|$ where ρ is the experimental density matrix and σ is the theoretical density matrix. So, fidelity is given by $F(\rho, \sigma) = \text{Tr}(\sqrt{\sqrt{\rho}\sigma\sqrt{\rho}})$. For any ρ and σ , $0 \leq F(\rho, \sigma) \leq 1$ and $F(\rho, \rho) = 1$. Also the fidelity has symmetric property i.e.

No. of Iteration	Fidelity using real chip	Fidelity using Simulator
1	0.1736	0.5275
5	0.4723	0.5614
10	0.4873	0.5759
15	0.4833	0.5827
20	0.4942	0.5858
25	0.5014	0.5915

TABLE I: Fidelity of real chip vs simulator

$F(\rho, \sigma) = F(\sigma, \rho)$. The measurement is done using X-basis, Y-basis and Z-basis using Santiago chip in IBMQ and QASM simulator for Fig: 4, the measurement of different iterations of above figure is also taken. The results is shown in the given table I, and plots in Fig: 15. Fidelity for classical simulator shows better results than the quantum real machine as can be seen from the graph, but the general growth pattern of fidelity is same for both Simulator and quantum real machine.

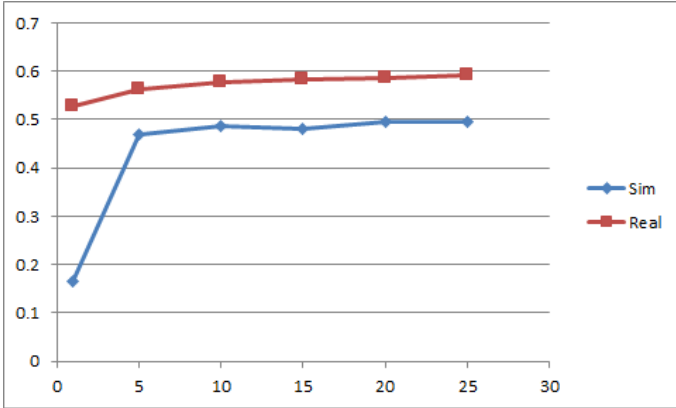


FIG. 15: Fidelity of real chip (ibmq Santiago) vs simulator of different iterations

VI. CONCLUSION

We have shown the basic circuit and simulation of the Ising-Hamiltonian which is the sum of all staggered energy and spin coupled complex of a dimer atomic lattice

with all the entangled states, for one dimensional dissipative spin chain in magnetic field. This particular case can be used as a test bed to understand steady state dynamics of dissipative spin chains for Hamiltonians of various models such as XXZ model, Heisenberg model⁶⁰ etc. We have mentioned about the time correlation factor of the synchronized state which weakly depend upon λ which could be calculated by measuring the average value, all the plots signify the time correlation factor and shows the spontaneous synchronization with the resonance peak⁵⁴ and could be further detected the relation between different energy and spin-spin coupling. But there are some points on the graph where each ω change its phase, where we would like to keep an open question about the behaviour of the ω in different θ value of λt , which would also depict the relationship between the one-time correlation operator with the synchronization states at particular ω and λt . We have also pointed out the anomalous behaviour of probabilities with respect to constant values of ω_1 which doesn't seem to follow a pattern, which may be used for further studies. We obtained lowest energy values for ground state energy for 24 layer and at 1st layer for first excited state for U3 anstaz while using SPSA optimizer, this gives a possibility of obtaining similar results using different anstaz and optimizers for far less number of layers in case of ground state energy which can be found using further studies of this field.

VII. ACKNOWLEDGEMENT

S.P., A.N., A.M., D.S., T.S.B. and S.K.S would like to thank Bikash's Quantum (OPC) Pvt. Ltd. for providing hospitality during the course of this project. B.K.B. acknowledges IISER-K Institute fellowship. The authors also acknowledge Victor Mukherjee and Rahul Sharma of IISER Berhampur who helped us the peer review respectively. S.P. and A.N. has contributed to the concept, theory, quantum circuit, VQE and the implementation part. D.S. and T.S.B has contributed to the graph plotting. S.K.S has contributed to the entire fidelity section and A.M has helped us in the literature writing of the paper. The authors appreciate IBM quantum experience's assistance in developing the fundamental circuits. The writers' opinions are their own and do not reflect IBM's or the IBM quantum experience team's official position.

VIII. REFERENCES

- ¹ Zhao-Chen Duan, Jin-Peng Li, Jian Qin, Ying Yu, Yong-Heng Huo, Sven Höfling, Chao-Yang Lu, Nai-Le Liu, Kai Chen, and Jian-Wei Pan, "Proof-of-principle demonstration of compiled Shor's algorithm using a quantum dot single-photon source," Opt. Express 28, 18917-18930 (2020)

* sudev18@iiserbpr.ac.in
† amlandeeep18@iiserbpr.ac.in
‡ sritam19@iiserbpr.ac.in
§ tanmaya18@iiserbpr.ac.in
¶ ankita18@iiserbpr.ac.in
** debashis18@iiserbpr.ac.in
†† bkb18rs025@iiserkol.ac.in

- ² B. P. Lanyon, T. J. Weinhold, N. K. Langford, M. Barbieri, D. F. V. James, A. Gilchrist, and A. G. White, Experimental Demonstration of a Compiled Version of Shor's Algorithm with Quantum Entanglement, *Phys. Rev. Lett.* **99**, 250505
- ³ Stephen B. Deutsch, John J. Martin, (1971) An Ordering Algorithm for Analysis of Data Arrays. *Operations Research* **19**(6):1350-1362.
- ⁴ Nagata, K., Nakamura, T. and Farouk, A. Quantum Cryptography Based on the Deutsch-Jozsa Algorithm. *Int J Theor Phys* **56**, 2887–2897 (2017)
- ⁵ Gulde, S., Riebe, M., Lancaster, G. et al. Implementation of the Deutsch–Jozsa algorithm on an ion-trap quantum computer. *Nature* **421**, 48–50 (2003). <https://doi.org/10.1038/nature01336>
- ⁶ Patrick Shea, Brandon P. van Zyl and Rajat K. Bhaduri, The two-body problem of ultra-cold atoms in a harmonic trap, *American Journal of Physics* **77**, 511 (2009)
- ⁷ J. Wehr, A. Niederberger, L. Sanchez-Palencia, and M. Lewenstein, Disorder versus the Mermin-Wagner-Hohenberg effect: From classical spin systems to ultracold atomic gases, *Phys. Rev. B* **74**, 224448 – Published 29 December 2006
- ⁸ M.A Baranov, Theoretical progress in Many Body Physics with Ultracold Dipolar Gases, *Physics Reports* **464**, 71-111 (2008).
- ⁹ Arpan Bhattacharyya, Alexander Jahn, Tadashi Takayanagi, and Koji Umemoto, Entanglement of Purification in Many Body Systems and Symmetry Breaking, *Phys. Rev. Lett.* **122**, 201601 – Published 22 May 2019
- ¹⁰ Wen Wei Ho, Soonwon Choi, Hannes Pichler, and Mikhail D. Lukin, Periodic Orbits, Entanglement, and Quantum Many-Body Scars in Constrained Models: Matrix Product State Approach, *Phys. Rev. Lett.* **122**, 040603 – Published 29 January 2019
- ¹¹ Jens H. Bardarson, Frank Pollmann, and Joel E. Moore, Unbounded Growth of Entanglement in Models of Many-Body Localization, *Phys. Rev. Lett.* **109**, 017202 – Published 3 July 2012
- ¹² A Cervera-Lierta, Exact Ising model simulation on a quantum computer, *Quantum* **2** **114**(2018)
- ¹³ Xun Gao, Sheng-Tao Wang, and L.-M. Duan, Quantum Supremacy for Simulating a Translation-Invariant Ising Spin Model, *Phys. Rev. Lett.* **118**, 040502 – Published 27 January 2017
- ¹⁴ Tai Tsun Wu, Barry M. McCoy, Craig A. Tracy, and Eytan Barouch, Spin-spin correlation functions for the two-dimensional Ising model: Exact theory in the scaling region, *Phys. Rev. B* **13**, 316 – Published 1 January 1976
- ¹⁵ Jiahui Chen, Hui Zhou, Changkui Duan, and Xinhua Peng-Preparing Greenberger-Horne-Zeilinger and W states on a long-range Ising spin model by global controls, *Phys. Rev. A* **95**, 032340 – Published 31 March 2017
- ¹⁶ T. Kaneyoshi, M. Jašćur, and I. P. Fittipaldi, Transverse Ising model with arbitrary spin, *Phys. Rev. B* **48**, 250 – Published 1 July 1993
- ¹⁷ T Plefka, Convergence condition of the TAP equation for the infinite-ranged Ising spin glass model, 1982 *J. Phys. A: Math. Gen.* **15** 1971
- ¹⁸ H.M. Babujian, Exact solution of the one-dimensional isotropic Heisenberg chain with arbitrary spins S, *Physics Letters A*, Volume 90, Issue 9,
- ¹⁹ U. Löw, V. J. Emery, K. Fabricius, and S. A. Kivelson, Study of an Ising model with competing long- and short-range interactions, *Phys. Rev. Lett.* **72**, 1918 – Published 21 March 1994
- ²⁰ J F Nagle, and, and J C Bonner, Phase Transitions-Beyond the Simple Ising Model, *Annual Review of Physical Chemistry* **1976** **27**:1, 291-317
- ²¹ Nicolas Höft, Jürgen Horbach, Victor Martín-Mayor and Beatriz Seoane, An Ising model for metal-organic frameworks, *Journal of Chemical Physics*, Issue **8** **147**, (20017).
- ²² Marc Weber and Javier Buceta, The cellular Ising model: a framework for phase transitions in multicellular environments, *Royal Society*, Volume **13** **119**
- ²³ Binder, K. Kinetic ising model study of phase separation in binary alloys. *Z. Physik* **267**, 313–322 (1974)
- ²⁴ G. R. Andersen and J. C. Wheeler, Two-component lattice-gas model with a liquid-vapor phase transition in both pure components, *J. Chem. Phys.* **70**, 1326 (1979).
- ²⁵ A. Pikovsky, M. Rosenblum, and J. Kurths, Synchronization: A Universal Concept in Nonlinear Sciences, *Phys. Tod.* **56**, 47 (2003).
- ²⁶ S. Rankovic, Y.-C. Liang, and R. Renner, Quantum clocks and their synchronisation - the Alternate Ticks Game, *arXiv:1506.01373*
- ²⁷ E. O. Ilo-Okeke, L. Tessler, J. P. Dowling and T. Byrnes, Remote quantum clock synchronization without synchronized clocks, *npj Quantum Inf.* **4**, 40 (2018).
- ²⁸ A. Cabot, G. L. G. F. Galve, and R. Zambrini, Quantum Synchronization in Dimer Atomic Lattices, *Phys. Rev. Lett.* **123**, 023604 (2019).
- ²⁹ L.-M. Duan, E. Demler, and M. D. Lukin, Controlling Spin Exchange Interactions of Ultracold Atoms in Optical Lattices, *Phys. Rev. Lett.* **91**, 090402 (2003). A. Imambekov, M. Lukin, and E. Demler, Spin-exchange interactions of spin-one bosons in optical lattices: Singlet, nematic, and dimerized phases, *Phys. Rev. A* **68**, 063602 (2003).
- ³⁰ I. R. Bonifacio, P. Schwendimann, and Fritz Haake, Quantum Statistical Theory of Superradiance, *Phys. Rev. A* **4**, 302 (1971).
- ³¹ Dmitry A. Fedorov, Bo Peng, Niranjana Govind and Yuri Alexeev, VQE Method: A Short Survey and Recent Developments, *arXiv:2103.08505v2* **quant-ph**
- ³² Aaron C. West, Michael W. Schmidt, Mark S. Gordon, and Klaus Ruedenberg, A comprehensive analysis of molecule-intrinsic quasi-atomic, bonding, and correlating orbitals. I. Hartree-Fock wave functions, *J. Chem. Phys.* **139**, 234107 (2013)
- ³³ Riccardo Borghi, The variational method in quantum mechanics: an elementary introduction, *European Journal of Physics*, **39**, 035410 (2018)
- ³⁴ H. Schwager, J. I. Cirac, and G. Giedke, Dissipative spin chains: Implementation with cold atoms and steady-state properties, *Phys. Rev. A* **87**, 022110 (2013).
- ³⁵ C.-C. Liu, H. Jiang, and Y. Yao, Low-energy effective Hamiltonian involving spin-orbit coupling in silicene and two-dimensional germanium and tin, *Phys. Rev. B* **84**, 195430 (2011).
- ³⁶ Philippe Pellegrini, Stephane Vranckx and Michèle Desouter-Lecomte, Implementing quantum algorithms in hyperfine levels of ultracold polar molecules by optimal control, *Phys. Chem. Chem. Phys.*, 2011, **13**, 18864-18871.
- ³⁷ T. T. Wu, B. M. McCoy, C. A. Tracy, and E. Barouch, Spin-spin correlation functions for the two-dimensional Ising model: Exact theory in the scaling region, *Phys. Rev.*

- B **13**, 316 (1976).
- ³⁸ J. F. Sherson, C. Weitenberg, M. Endres, M. Cheneau, I. Bloch and S. Kuhr, Single-atom-resolved fluorescence imaging of an atomic Mott insulator, *Nature* **467**, 68-72 (2010).
 - ³⁹ C. Maschler and H. Ritsch, Cold Atom Dynamics in a Quantum Optical Lattice Potential, *Phys. Rev. Lett.* **95**, 260401 (2005).
 - ⁴⁰ Heike Schwager, J. Ignacio Cirac, and Géza Giedke, Dissipative spin chains: Implementation with cold atoms and steady-state properties, *Phys. Rev. A* **87**, 022110 – Published 13 February 2013
 - ⁴¹ Albert Cabot, Gian Luca Giorgi, Fernando Galve, and Roberta Zambrini, Quantum Synchronization in Dimer Atomic Lattices, *Phys. Rev. Lett.* **123**, 023604 – Published 9 July 2019
 - ⁴² Xingcan Dai, Eliza-Beth W. Lerch, and Stephen R. Leone, Coherent control through near-resonant Raman transitions, *Phys. Rev. A* **73**, 023404 – Published 6 February 2006
 - ⁴³ C. C. Marston and G. G. Balint-Kurti, The Fourier grid Hamiltonian method for bound state eigenvalues and eigenfunctions, *J. Chem. Phys.* **91**, 3571 (1989).
 - ⁴⁴ N. Zagury, A. Aragão, J. Casanova, and E. Solano, Unitary expansion of the time evolution operator, *Phys. Rev. A* **82**, 042110 – Published 21 October 2010; Erratum *Phys. Rev. A* **84**, 019903 (2011)
 - ⁴⁵ H. Araki, Hamiltonian Formalism and the Canonical Commutation Relations in Quantum Field Theory, *J. Math. Phys.* **1**, 492 (1960)
 - ⁴⁶ Ho Lun Tang, V.O. Shkolnikov, George S. Barron, Harper R. Grimsley, Nicholas J. Mayhall, Edwin Barnes, and Sophia E. Economou, Qubit-ADAPT-VQE: An Adaptive Algorithm for Constructing Hardware-Efficient Ansätze on a Quantum Processor, *PRX Quantum* **2**, 020310 – Published 28 April 2021
 - ⁴⁷ X.-L. Deng, D. Porras, and J. I. Cirac, Effective spin quantum phases in systems of trapped ions, *Phys. Rev. A* **72**, 063407 – Published 19 December 2005
 - ⁴⁸ Sangchul Oh, Soonchil Lee, and Hai-woong Lee, Fidelity of quantum teleportation through noisy channels *Phys. Rev. A* **66**, 022316 – Published 27 August 2002
 - ⁴⁹ Mathias Soeken, D. Michael Miller, and Rolf Drechsler, Quantum circuits employing roots of the Pauli matrices, *Phys. Rev. A* **88**, 042322 – Published 16 October 2013
 - ⁵⁰ Kim, T. q-Extension of the Euler formula and trigonometric functions. *Russ. J. Math. Phys.* **14**, 275–278 (2007)
 - ⁵¹ Shuhei Tamate, Kazuhisa Ogawa, and Masao Kitano, Bloch-sphere representation of three-vertex geometric phases, *Phys. Rev. A* **84**, 052114 – Published 21 November 2011
 - ⁵² R. J. Baxter, Corner transfer matrices of the eight-vertex model. II. The Ising model case, *J. Stat. Phys.* **17**, 1-14 (1977).
 - ⁵³ I. Steiner and P. E. Toschek, Quenching Quantum Phase Noise: Correlated Spontaneous Emission versus Phase Locking, *Phys. Rev. Lett.* **74**, 4639 (1995).
 - ⁵⁴ H. J. Schulz, Phase diagrams and correlation exponents for quantum spin chains of arbitrary spin quantum number, *Phys. Rev. B* **34**, 6372 – Published 1 November 1986
 - ⁵⁵ S. Walter, A. Nunnenkamp, and C. Bruder, Quantum Synchronization of a Driven Self-Sustained Oscillator, *Phys. Rev. Lett.* **112**, 094102 (2014).
 - ⁵⁶ F Igloi et al 1983 *J. Phys. A: Math. Gen.* **16** 4067
 - ⁵⁷ Peruzzo, A., McClean, J., Shadbolt, P. et al. A variational eigenvalue solver on a photonic quantum processor. *Nat Commun* **5**4213 (2014)
 - ⁵⁸ Salonik Resch, Introductory Tutorial for SPSA and the Quantum Approximation Optimization Algorithm, [arXiv:2106.01578v1](https://arxiv.org/abs/2106.01578v1) [**quant-ph**]
 - ⁵⁹ Amaran, S., Sahinidis, N.V., Sharda, B. et al. Simulation optimization: a review of algorithms and applications. *4OR-Q J Oper Res* **12** 301–333 (2014).
 - ⁶⁰ Sergei Lukyanov, Low energy effective Hamiltonian for the XXZ spin chain, *Nuclear Physics B*, Volume 522, Issue 3, (1998), 533-549,